Journal of Geochemical Exploration 140 (2014) 64–76

Contents lists available at ScienceDirect

Journal of Geochemical Exploration

journal homepage: www.elsevier.com/locate/jgeoexp

Delineation of alteration zones based on Sequential Gaussian Simulation and concentration–volume fractal modeling in the hypogene zone of Sungun copper deposit, NW Iran

Fatemeh Soltani [a,*], Peyman Afzal [a,b], Omid Asghari [c]

[a] Department of Mining Engineering, Faculty of Engineering, South Tehran Branch, Islamic Azad University, Tehran, Iran
[b] Camborne School of Mines, University of Exeter, Penryn, UK
[c] Simulation & Data Processing Laboratory, Department of Mining Engineering, University of Tehran, Tehran, Iran

ARTICLE INFO

Article history:
Received 23 July 2013
Accepted 9 February 2014
Available online 18 February 2014

Keywords:
Sequential Gaussian Simulation (SGS)
Concentration–volume (C–V) fractal model
Alteration zones
Sungun Cu porphyry deposit
Geostatistics

ABSTRACT

The main aim of this study is the identification of potassic, phyllic and propylitic alteration zones in the hypogene zone of the Sungun Cu porphyry deposit (NW Iran) based on drillcore data, utilizing sequential geostatistical simulation (SGS) and concentration–volume (C–V) fractal model. C–V log–log plots were generated for the results obtained by 10 realizations and the average of those realizations (E-type) which was used for the determination of Cu threshold values for the alteration zones. Based on correlation between geological models and the results derived via SGS and C–V fractal modeling by log ratio matrix, the propylitic zone has Cu values < 0.005% as a result of simulation numbers (sims) 1, 5 and 9 with overall accuracy (OA) of 0.94. Additionally, the phyllic alteration contents of Cu values between 0.25% and 0.63% with OA of 0.70 are delineated by E-type. Moreover, a correlation between C–V fractal modeling of realizations and the potassic alteration zone derived via the geological model reveals that this alteration zone has Cu values higher than 2.23% (sims 1, 5 and 9) with OA of 0.816. The results of this research reveal that phyllic alteration due to having many existing geological samples with the grades close to the average ore grade (0.44%) of the Sungun deposit has a proper overlap with E-type; however, potassic and propylitic alterations containing the highest and lowest ore grades have a strong overlap with sims 1, 5 and 9.

1. Introduction

Different alteration patterns and their spatial variability have vital roles in grade distribution within an ore deposit. In the other hand, the grade variability would be affected by rock type and alteration changes. For better understanding of these grade dependent processes, it is very important to predict the spatial distribution of the grade within the desired ore deposit (Asghari and Hezarkhani, 2008). Conventional methods to distinguish alteration zones in hydrothermal deposits are based on mineralogical, petrographical and geochemical investigations including assemblages of minerals and ore mineral recognition utilizing thin sections, X-Ray Diffraction (XRD), Electron Probe Micro Analyzer (EPMA), Scanning Electron Microscopy (SEM) and Portable Infrared Mineral Analyzer (PIMA: e.g., Berger et al., 2008; Chouinard et al., 2005; Cox and Singer, 1986; Hedenquist et al., 2000; Hoefs, 2009; Lowell and Guilbert, 1970; Pirajno, 2009; Richards, 1995; Sillitoe, 1997).

Geostatistics has been used for spatial variability characterization and prediction of grade over the last three decades. Ordinary kriging (OK) is the most useful geostatistical estimation technique which is also called the "best linear unbiased estimator" (Isaaks and Srivastava, 1989; Journel and Huijbregts, 1978). The most important negative characteristics of moving average estimators such as kriging are smoothing effect and reducing the range of variation of the variables. Geostatistical simulation is widely used to overcome this problem and avoiding the smoothing effect of such estimation methods (Chilès and Delfiner, 2012).

Geostatistical stochastic simulations have the ability not only to estimate the spatial distribution of the regionalized variable but also to assess both local uncertainty and spatial uncertainty about the estimates (Deutsch and Journel, 1998; Goovaerts, 1997). Conditional stochastic simulation is designed initially to overcome the smoothing effect of kriging estimator especially when mapping sharp or extreme spatial discontinuities are to be found (Deutsch and Journel, 1998; Leuangthong et al., 2004).

The simulation algorithms take into account both the spatial variation of actual data at sampled locations and on the other hand, the variation of estimates at unsampled locations (Delbari et al., 2009). It means that stochastic simulation reproduces the sample statistics (histogram and semi-variogram model) and honors the sample data at their original locations. Therefore a stochastic simulation map represents the spatial distribution of a more realistic attribute than a kriged map (Asghari and Madani Esfahani, 2013; Rezaee et al., 2013).

* Corresponding author.
E-mail address: fsoltani1390@gmail.com (F. Soltani).

http://dx.doi.org/10.1016/j.gexplo.2014.02.007
0375-6742/

Many stochastic simulation algorithms have been proposed and among them Sequential Gaussian Simulation (SGS) is widely used because it is fast and straightforward in reconstructing conditional cumulative distribution function (CCDF: Chen et al., 2013; Geboy et al., 2013; Maleki Tehrani et al., 2012; Manchuk and Deutsch, 2012a, 2012b).

In most interpolation algorithms such as OK, the aim is to provide the "best" local estimation of the variables without consideration of spatial conditions. The whole point of geostatistical simulation is to reproduce the variance of the input data, both in a univariate (histogram) and spatial (variogram) sense. Consequently, simulations provide an appropriate platform to study any problem relating to variability (Goovaerts, 1996).

Kriging is used for the local set of data and conditional statistics as an interpolation method which gives a simple numerical method in the sense of local precision. Simulation provides several alternatives but equally probable models all of which are the "best" reflection of the reality in a certain global sense. The differences between the realizations offer an opportunity for measuring the spatial uncertainty (Goovaerts, 1996; Ravenscroft, 1994).

The geostatistical simulation methods employ simple kriging at a voxel to estimate the posterior mean and variance, with random sampling of the posterior distribution to create a realization at the corresponding voxels (Dimitrakopoulos and Luo, 2004; Ravenscroft, 1994).

Fractal/multifractal modeling, established originally by Mandelbrot (1983), has been widely applied for separating the different geological/mineralization processes. Variation of geochemical and mineralization processes can be explained based on differences in fractal dimensions obtained from analysis of relevant geochemical data (Afzal et al., 2011, 2012; Cheng et al., 1994; Goncalves et al., 2001; Sim et al., 1999; Wang et al., 2011; Yasrebi et al., 2013). Models of fractal/multifractal analysis also serve to reveal the relationships of geological, geophysical, geochemical and mineralogical settings with spatial information derived via analysis of mineral deposit data (Afzal et al., 2011; Carranza, 2009; Daneshvar Saein et al., 2012; Goncalves et al., 2001; Gumiel et al., 2010). However, good knowledge of geological environmental controls on mineralization (e.g., alteration zones) is important in the identification and classification of geochemical populations based on fractal/multifractal models (Afzal et al., 2011, 2013; Arias et al., 2012; Carranza and Sadeghi, 2010; Cheng, 1999; Delavar et al., 2012; Li et al., 2003; Sadeghi et al., 2012; Sim et al., 1999; Yasrebi et al., 2013; Zuo, 2011; Zuo et al., 2009).

Fractal dimensions in geological and mineralization processes correspond to variations in physical characteristics such as rock type, fluid phase, alteration zones, vein density or orientation, and structural feature or dominant mineralogy (i.e., Afzal et al., 2011; Sim et al., 1999). In recent years, fractal/multifractal modeling has been utilized for delineation of mineralized zones in different types of ore deposits such as number–size (N–S: Mandelbrot, 1983), size–grade (S–G: Agterberg, 1995), concentration–volume (C–V: Afzal et al., 2011), power spectrum–volume (P–V: Afzal et al., 2012) and concentration–number (C–N: Hassanpour and Afzal, 2013).

Different geochemical processes can be defined based on variations in fractal dimensions derived via analysis of relevant geochemical data. Fractal dimensions in geological and geochemical processes correspond to differences in physical characteristics such as lithology, vein density or orientation, fluid phase, alteration phenomena, and structural feature or dominant mineralogy (Afzal et al., 2011; Sim et al., 1999; Yasrebi et al., 2013). Conventional models based upon geological studies and analysis of cores from boreholes with the purpose of delineating the mineralized zones do not have a high efficiency in the ore deposits especially in the porphyry deposits. The fractal/multifractal modeling has a distinctive power to distinguish the natural populations like different ore grades within a deposit (Yasrebi et al., 2013).

In this paper, Sequential Gaussian Simulation (SGS) and C–V fractal modeling were utilized for delineating various alteration zones (potassic, phyllic and propylitic) based on Cu values in the hypogene zone of Sungun Cu porphyry deposit, NW Iran.

2. Geological setting

Main porphyry copper mineralization in Iran occurs in the Cenozoic Sahand–Bazman orogenic belt (Fig. 1). The Sahand–Bazman belt was formed by subduction of the Arabian plate beneath central Iran during the Alpine orogeny. Subduction caused extensive alkaline and calc-alkaline volcanic and plutonic igneous activities, including intrusion of a porphyritic calc-alkaline stock at Sungun during Miocene times (Berberian and King, 1981; Dargahi et al., 2010; Mehrpartou, 1993).

The Sungun porphyry copper deposit (PCD) is located about 100 km NE of Tabriz, NW Iran (Fig. 1). The Sungun deposit is hosted by diorite/granodiorite to monzonite/quartz–monzonite stocks (Hezarkhani, 2006; Mehrpartou, 1993). The porphyry stock II (which is studied in this research) hosts the Sungun PCD and varies in composition from quartz monzonite through granodiorite to granite. Four series of dikes injected lately varying in composition from quartz monzodiorite to granodiorite intersect the Sungun stocks (Calagari, 2004).

The NNW–SSE trending dykes dip steeply to the west and have thickness from a few centimeters to several tens of meters (Fig. 1: Asghari et al., 2009; Rashidinejad et al., 2008).

3. Alteration and mineralization

Different alterations and related mineralization in the Sungun PCD have been studied by geological investigations (Asghari et al., 2009; Hezarkhani, 2006; Mehrpartou, 1993). Hydrothermal alteration and mineralization at Sungun are centered on the porphyry stock II. An early hydrothermal alteration was dominantly potassic and propylitic, and it was followed later by phyllic and argillic alterations (Asghari et al., 2009; Hezarkhani and Williams-Jones, 1998).

3.1. Potassic alteration

The earliest alteration is represented by potassic mineral assemblages developed pervasively and as halos around veins in the deep and central parts of the Sungun stock. Potassic alteration is characterized by the occurrence of K-feldspar and displays a close spatial association with copper and molybdenum mineralization (Hezarkhani et al., 1999; Mehrpartou, 1993).

3.2. Phyllic alteration

Phyllic alteration is characterized by the replacement of almost all rock-forming silicates by sericite and quartz and overprints the earlier formed potassic. Pyrite forms up to 5 vol.% of the rock and occurs in veins and disseminations. Quartz veins are surrounded by weak sericitic halos. Vein-hosted pyrite is partially replaced by chalcopyrite. Silicification was synchronous with phyllic alteration and variably affected much of the stock and most dikes (Asghari et al., 2009; Hezarkhani, 2006).

3.3. Propylitic

Propylitic alteration is characterized by the chloritization of primary and secondary biotite, amphibole and groundmass materials in rocks peripheral to the central potassic zone. Minor minerals associated with propylitic alteration are albite, calcite, sericite, anhydrite (gypsum), and pyrite. The propylitic type of alteration is restricted to peripheral porphyry stocks and some dike series (Calagari, 2004).

3.4. Argillic

Within some areas, 80 m of the erosional surface of the entire rock has been altered to an assemblage of clay minerals, hematite

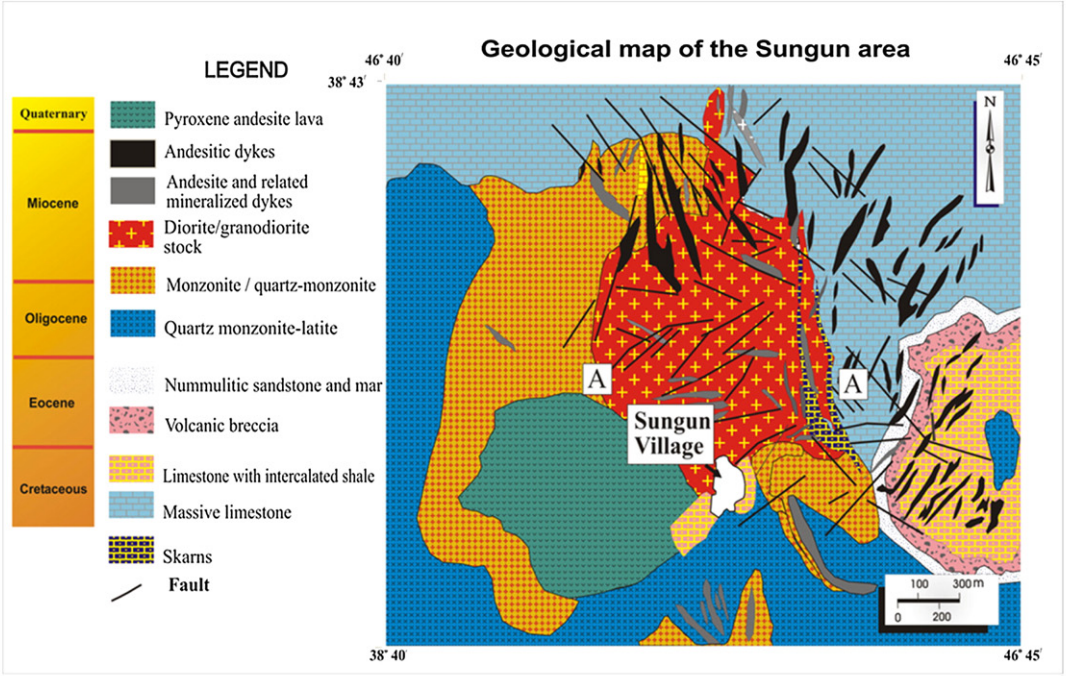
Geological map of the Sungun area
LEGEND
Quaternary
Miocene
Oligocene
Eocene
Cretaceous
Pyroxene andesite lava
Andesitic dykes
Andesite and related mineralized dykes
Diorite/granodiorite stock
Monzonite / quartz-monzonite
Quartz monzonite-latite
Nummulitic sandstone and mar
Volcanic breccia
Limestone with intercalated shale
Massive limestone
Skarns
Fault
46° 40′
38° 43′
46° 45′
38° 40′
N
A
A
Sungun Village
100 300 m
0 200

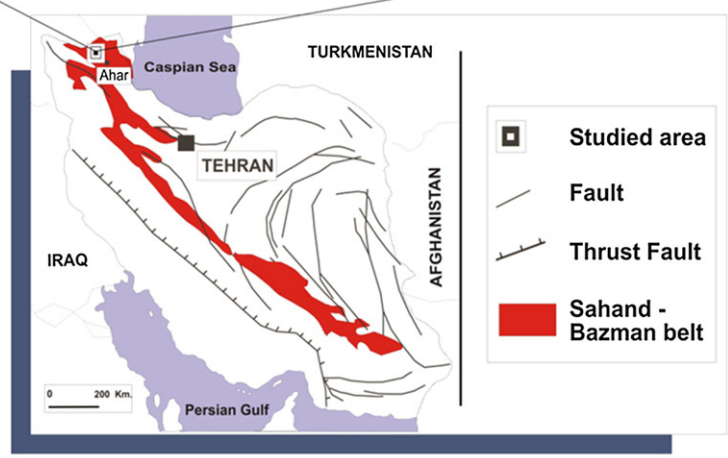
Ahar
Caspian Sea
TURKMENISTAN
TEHRAN
IRAQ
AFGHANISTAN
Persian Gulf
0 200 Km.
Studied area
Fault
Thrust Fault
Sahand - Bazman belt

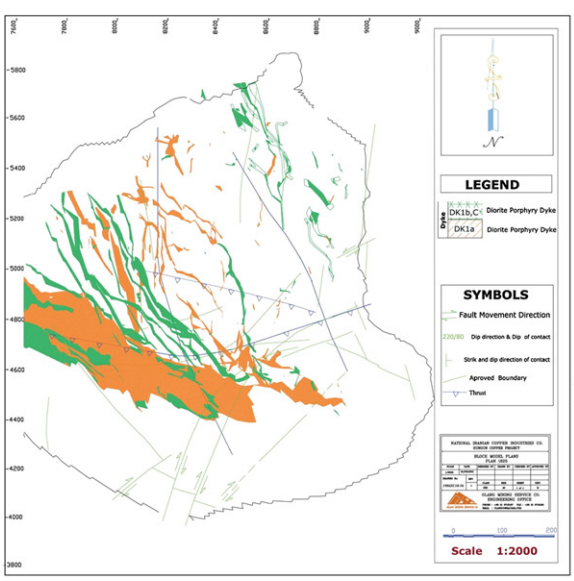
LEGEND
Dike
DK1b,C
Diorite Porphyry Dyke
DK1a
Diorite Porphyry Dyke
SYMBOLS
Fault Movement Direction
Dip direction & Dip of contact
Strik and dip direction of contact
Aproved Boundary
Thrust
Scale 1:2000

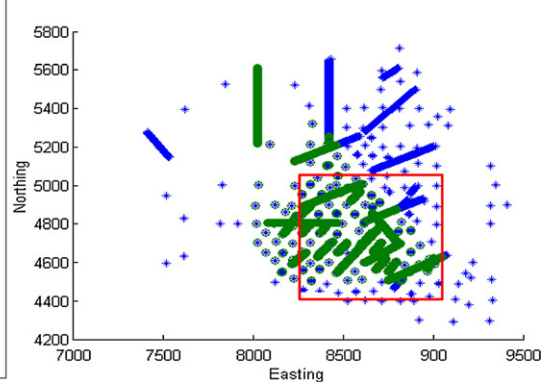
Northing
Easting
5800
5600
5400
5200
5000
4800
4600
4400
4200
7000
7500
8000
8500
900
9500

Table 1
Basic statistics of Cu raw data (n = 19,605) and output grid for different realizations, E-type and ordinary kriging.

	Range (%)	Min (%)	Max (%)	Mean (%)	Var ($\%^2$)	Skewness
Raw data	6.999875	0.000125	7	0.445	0.226	1.47
sim 1	5.5103	0.0002	5.5	0.47	0.245	1.354
sim 2	6.1	0	6.1	0.46	0.234	1.331
sim 3	6.7997	0.0003	6.8	0.47	0.237	1.237
sim 4	6.299	0.001	6.3	0.46	0.226	1.196
sim 5	6.5996	0.0004	6.6	0.45	0.22	1.232
sim 6	6.699	0.001	6.7	0.48	0.243	1.224
sim 7	5.2999	0.0001	5.3	0.46	0.246	1.475
sim 8	5.4998	0.0002	5.5	0.46	0.236	1.4
sim 9	4.4995	0.0005	4.5	0.48	0.243	1.277
sim 10	3.3995	0.0005	3.4	0.46	0.232	1.239
E-type	2.0775	0.0025	2.08	0.44	0.063	0569
Kriged	4.11	0	4.11	0.46	0.232	0.29

and quartz but feldspar is altered to clay locally to a depth of about 400 m. A shallow level of alteration is interpreted to represent a supergene blanket over the deposit and the deeper clay alteration of feldspar may represent an advanced argillic stage of the hypogene alteration. Most samples taken from argillic alteration averaging 0.09% Cu content demonstrate that this barren zone could be assumed as waste from an exploitation point of view (Asghari et al., 2009).

3.5. Supergene enrichment

Two distinct supergene enrichment mineralized zones are recognized at Sungun (1) oxidized and leached zone and (2) supergene sulfide zone. The thickness of the supergene zone is non-uniform and it could be seen that the eastern part contains higher thickness and Cu grade compared to the western part. This can be structurally controlled by numerous NEE and NWW-trending faults. Meteoritic water leaches the copper from the oxide zone and while passing the faults beneath the water table, precipitates the copper in the form of native copper and secondary sulfides. Supergene enrichment zone determined by geological studies indicates the presence of chalcocite, chrysocolla, azurite, malachite and digenite (Asghari et al., 2009; Parsolang report, 2006).

3.6. Hypogene zone

Hypogene copper mineralization was introduced during potassic alteration and to a more extent during phyllic alteration (Asghari and Hezarkhani, 2008). During potassic alteration, the copper mineralization was deposited as chalcopyrite and minor bornite; later hypogene copper mineralization deposited mainly chalcopyrite. Alteration of feldspars and biotite (from potassically altered rocks) was accompanied by an increase in sulfide content outward from the central part of the stock. The maximum Cu grade is associated with biotite, orthoclase, and sericite (potassic zone) while the pyrite content is highest (3–10 vol.% of the rock) in the marginal quartz–sericite (phyllic) zone (Hezarkhani and Williams-Jones, 1998).

4. Methodology

4.1. Sequential Gaussian Simulation (SGS)

Sequential simulation is a stochastic modeling algorithm that obtains multiple realizations based on the same input data (Geboy et al., 2013; Journel, 1993). This data could be either continuous or categorical. Regarding the data type, sequential indicator simulation, Sequential Gaussian Simulation (SGS: Isaaks and Srivastava, 1989; Qu et al., 2013) or direct sequential simulation will be used.

The most straightforward algorithm for generating realizations of a multivariate Gaussian field is provided by the sequential principle (Leuangthong et al., 2004; Manchuk and Deutsch, 2012a, 2012b). SGS demands standard Gaussian data with zero mean and unit variance, so for SGS, data are transformed to be Gaussian through a quantile transformation (Chilès and Delfiner, 2012). Each variable is simulated sequentially according to its normal CCDF through a simple kriging

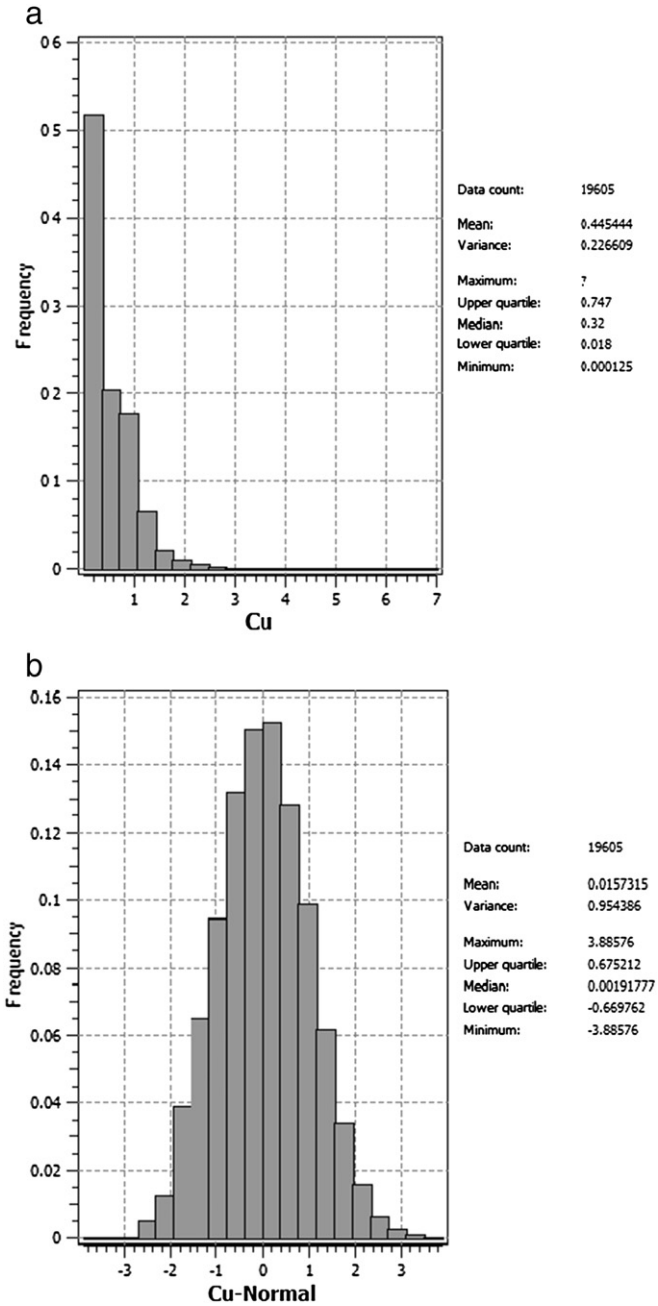

Fig. 2. Histogram of the raw (a) and normal score transformed (b) data.

Fig. 1. Geological map of the Sungun PCD and its location in the Sahand–Bazman belt which shows the field relationships among the various subtypes of Sungun intrusive rocks and the outline of the mineralized zone (modified from Asghari et al., 2009 and Hezarkhani, 2006), dyke series DK1a and DK1b&c (upper right) and drilling grid of the area (the red rectangle having the highest density of drill holes was selected for this study).

estimation system. The conditioning data consist of all original data and all previously simulated values found within a neighborhood of the location being simulated (Leuangthong et al., 2004; Manchuk and Deutsch, 2012a, 2012b).

The conditional simulation of a *continuous* variable z(u) in a Gaussian space proceeds as follows (Zanon and Leuangthong, 2004):

1 define a stationary domain.

2 draw the univariate Cumulative Distribution Function (CDF) of the domain after having done the declustering if the data are not in a regular grid.
3 transform the z data into y (a standard normal) using the CDF Fz(z).
4 Draw a random path which meets all nodes of the grid in each realization. At each node (u):

   a. define a search ellipsoid to find adjacent data and previously simulated values,
   b. use SK with the normal score variogram model to determine the mean and variance of the CCDF of the RF Y(u) at location u.
   c. perform Monte Carlo simulation to obtain a single value from the distribution (Zanon and Leuangthong, 2004).

5 add the simulated value to the data set
6 proceed to the next node, and loop until all nodes are simulated
7 backtransform the simulated normal values into the original unit (Deutsch and Journel, 1998).

Regarding a transformation to Gaussian and then backtransform to an original unit, statistical fluctuations are inherent in simulation but the fluctuations should be reasonable and unbiased in the mean and variance (Zanon and Leuangthong, 2004).

The following checks should be performed after having all nodes simulated: reproduction of (1) the data values at data locations, (2) the original histogram, (3) the original summary statistics, and (4) the input covariance model (Zanon and Leuangthong, 2004).

4.2. Concentration–volume fractal model

The C–V fractal model, which was proposed by Afzal et al. (2011) for delineation of mineralized zones and barren host rocks in porphyry-Cu deposits, can be expressed as:

$$V(\rho \leq \upsilon) \propto \rho^{-a1}; \quad V(\rho \geq \upsilon) \propto \rho^{-a2}$$

where $V(\rho \leq \upsilon)$ and $V(\rho \geq \upsilon)$ represent the two volumes with concentration values less than or equal to and greater than or equal to the contour value ρ; υ represents the threshold value of a geological zone (or volume); and a1 and a2 are the characteristic exponents. Threshold values in this model show boundaries between various mineralized (or alteration) zones of various mineral deposits. In this paper, $V(\rho \leq \upsilon)$ and $V(\rho \geq \upsilon)$ which are the volumes enclosed by a contour level ρ in a 3D model, the borehole data of ore concentrations were calculated by using SGS method.

5. Simulation of copper grade based on SGS

5.1. Descriptive statistics and spatial autocorrelation analysis

Descriptive statistics and the histogram of copper grades from 19,605 samples in the hypogene zone of the Sungun PCD are presented in Table 1 and Fig. 2, respectively which show the distribution of Cu data is not normal with the Cu mean value of 0.445%.

The Cu data have been transformed by using a normal score transformation and the statistics of transformed data (i.e. the mean value close to 0 and the variance of about 1) check the correctness of the transformation. The display of the histogram of new Gaussian variable also checks that the distribution is symmetric with minimum and maximum values of −3.88 and 3.88 respectively (Fig. 2). Geostatistical studies and visualizations were done with SGeMS and Datamine studios. An experimental semi-variogram and a spherical model fitted to the raw and normal transformed data are presented in Fig. 3.

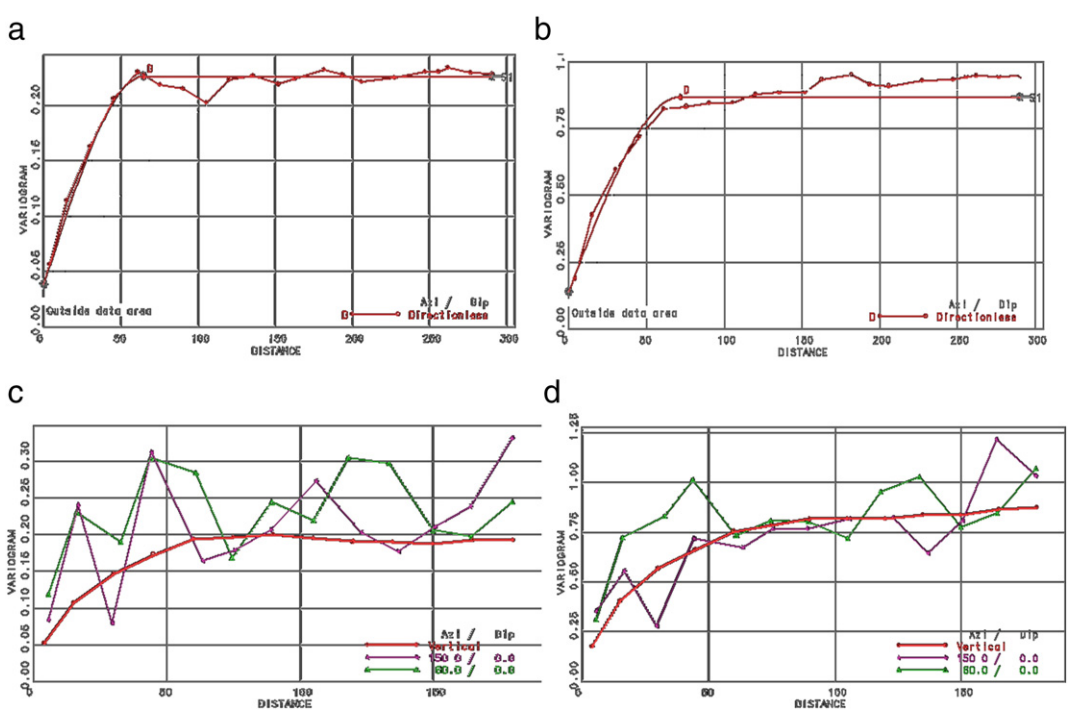

Fig. 3. Experimental semi-variograms and proper fitted model of the raw (a) and normal score transformed (b) data in the hypogene zone of the Sungun PCD and experimental directional semi-variograms of the raw (c) and normal score transformed (d) data for major and minor and vertical directions.

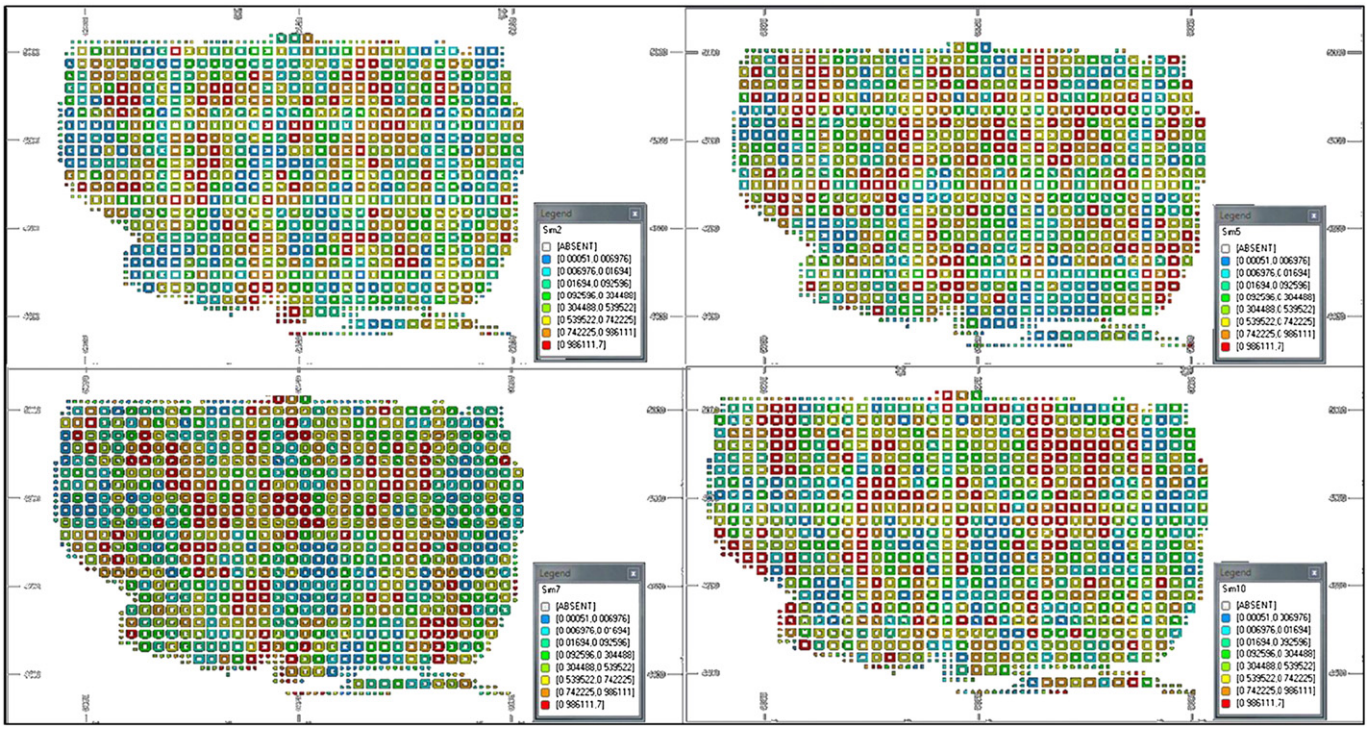

Fig. 4. Horizontal plan of four randomly selected realizations of the spatial distribution of Cu within the hypogene zone through applying SGS.

Anisotropy has also been investigated and modeled based on calculating the experimental semi-variograms of Cu and normalized value among horizontal directions with 30° angular increments and ± 15° angular tolerance and one vertical direction. The results show a mild anisotropy in the azimuth of 150 (major axis) for normal values, as depicted in Fig. 4.

The isotropic semi-variogram of raw data follows a spherical structure with a nugget effect of 0.038 $(\%)^2$ which reaches to a sill of 0.22 $(\%)^2$ at a range of 64.7 m, as shown in Fig. 3-a. The experimental semi-variogram of the normal scores (Fig. 3-b) follows again a spherical model with a nugget effect of 0.138 $(\%)^2$ with a range of spatial correlation about 71 m, which is similar to the one obtained for the raw data. That means the intrinsic spatial character of the Cu data does not vary with the normal transformation of data. The sill of the semi-variogram for the transformed data reaches to unity, as it should be to fulfill the second-order stationary assumption.

5.2. Conditional simulation

Based on SGS modeling, ten realizations of Cu spatial distributions are generated on a 25 × 25 × 25 (m^3) grid within the hypogene zone. Simulation is performed using the simple kriging estimator, and the semi-variogram model of Cu normal scores. Horizontal plan of four randomly selected realizations consisting of simulation numbers (sims 2, 5, 7 and 10) is displayed in Fig. 5. Each realization represents a realistic spatial distribution of Cu without a smoothing effect.

Four randomly selected realizations are checked to examine the sample statistics reproduction. The CDFs of all realizations of Cu distribution and also E-type and kriged map are displayed, as depicted in Fig. 6. Comparing these frequencies with the sample cumulative frequency (solid red line in the same shape) reveals that the realizations reproduce the sample histogram, reasonably well (Fig. 6). The reproduction of the Cu raw data semi-variogram model by selected realizations is also proper.

Some discrepancies between different realizations and sample models called ergodic fluctuations are acceptable which may have different reasons such as the algorithm used for the simulation, the semi-variogram model parameters and the amount of conditioning data to be utilized for the simulation (Goovaerts, 1997).

In the case of SGS algorithm, the histogram and semi-variogram models reproduced over a number of realizations should be, on average, equal to the sample statistics (Figs. 6 and 7: Emery and Peláez, 2012).

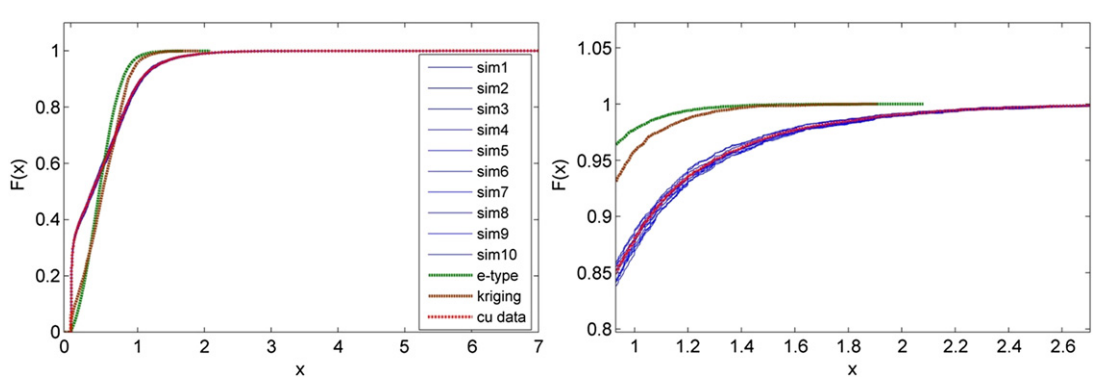

Fig. 5. CDF of all realizations reproduces the sample Cu histogram. CDF of kriging and E-type could not reproduce the sample data especially for high values as depicted in the right.

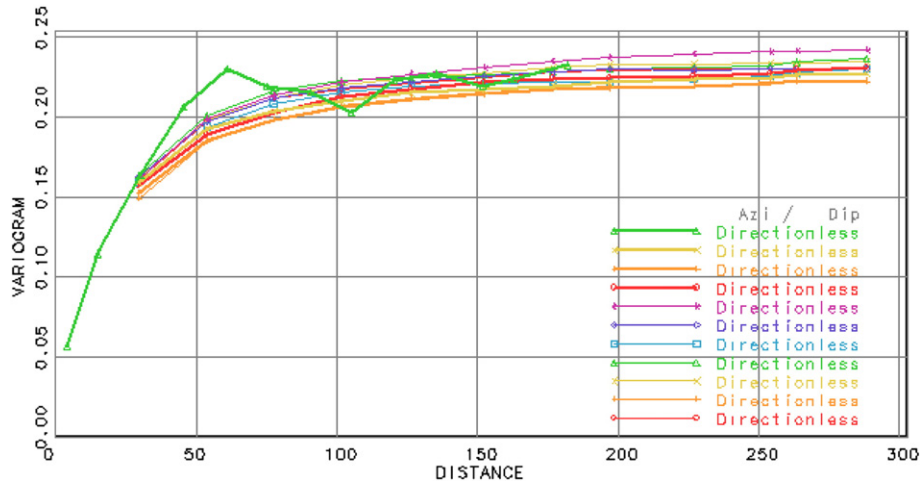

Fig. 6. Experimental semi-variogram of the 10 realizations compared to the sample data (green line). According to voxel size of 25 × 25 × 25 m the experimental semi-variogram of realizations could not find pairs for increments below 25 m.

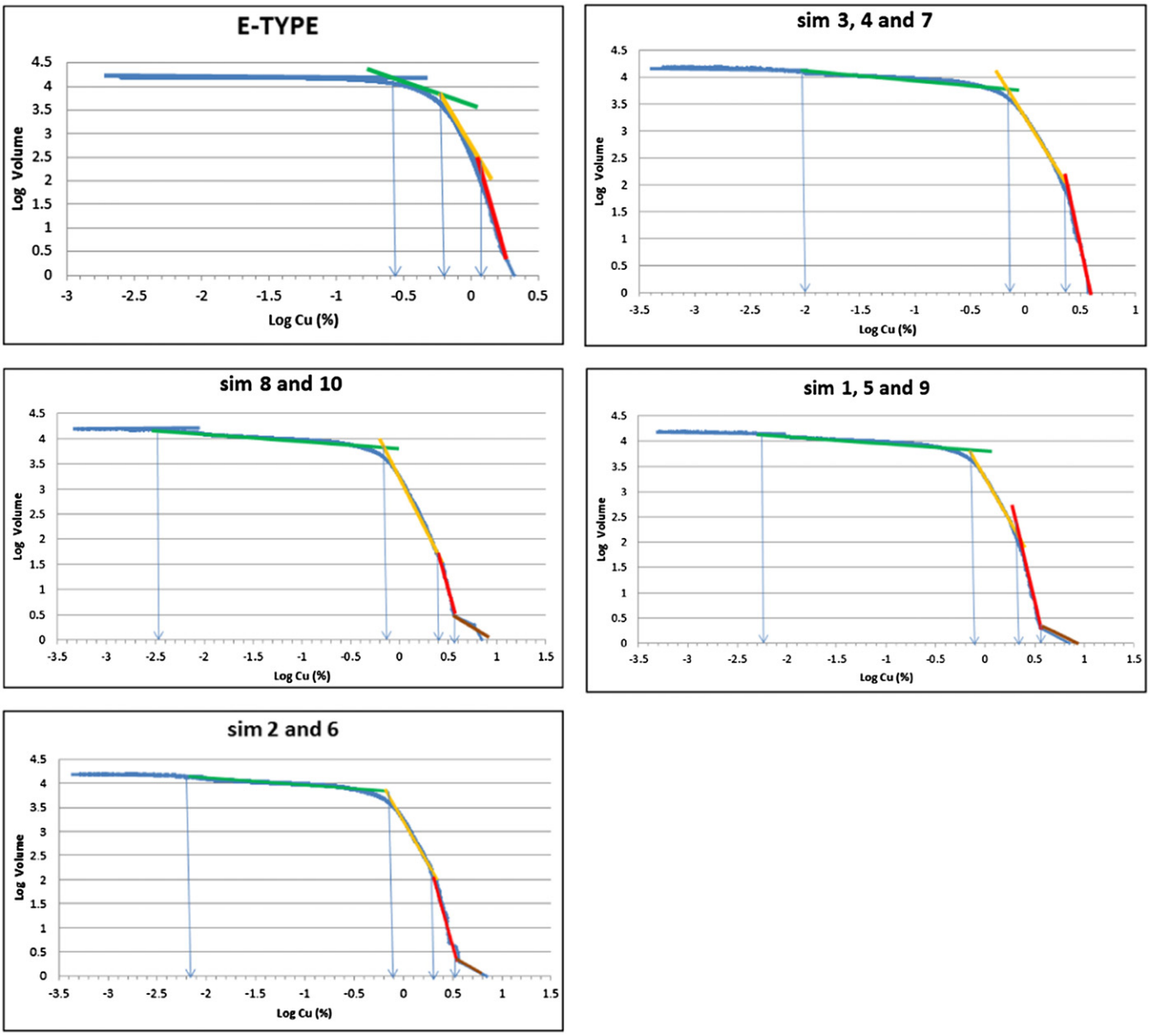

Fig. 7. Log–log plots of different realizations of SGS and E-type.

Table 2
Cu threshold values were recognized using C–V fractal model for different realizations and E-type.

Realization no.	First (%)	Second (%)	Third (%)	Fourth (%)
sim 1	0.005	0.79	2.23	3.54
sim 2	0.007	0.79	1.99	3.54
sim 3	0.01	0.7	2.23	–
sim 4	0.01	0.7	2.23	–
sim 5	0.005	0.79	2.23	3.54
sim 6	0.007	0.79	1.99	3.54
sim 7	0.01	0.7	2.23	–
sim 8	0.003	0.7	2.5	–
sim 9	0.005	0.79	2.23	3.54
sim 10	0.003	0.7	2.5	–
E-type	0.25	0.63	1.25	–

Each realization well preserves the range of variation of the measured Cu data compared to OK map which is illustrated in Table 2. This reveals the smoothing effect, a typical property of kriging. This is also evident from the kriging variance, which is much smaller than the actual variance. OK does not reflect the true variability especially for high values (Fig. 6), and hence is not appropriate for the underlying outlook to this study. Summary statistics of E-type estimate map are however similar to those for kriged map. On the other hand, results obtained by E-type have good correlations with estimation values derived via ordinary kriging.

6. C–V fractal modeling

Based on the results obtained from SGS, volumes corresponding to different Cu values were calculated to derive C–V fractal modeling. Threshold values of Cu are identified in the C–V log–log plots (Fig. 8), which indicate a power–law relationship between copper contents and volumes occupied in different realizations (Table 3). Based on the log–log plots, threshold values of Cu are similar in sims 3, 4 and 7 with three thresholds in 0.01%, 0.7% and 2.23% of Cu values. The log–log plots of sims 1, 5 and 9 show four threshold values which equal to 0.005%, 0.79%, 2.23% and 3.54%. However, log–log plots of sims 2 and 6 indicate four threshold values for Cu which are 0.007%, 0.79%, 1.99% and 3.54%. Additionally, three threshold values were defined in sims 8 and 10 in 0.003%, 0.7% and 2.5%. Moreover, the log–log plot for E-type illustrated three Cu threshold values in 0.25%, 0.63% and 1.25%, as depicted in Fig. 8 and Table 3.

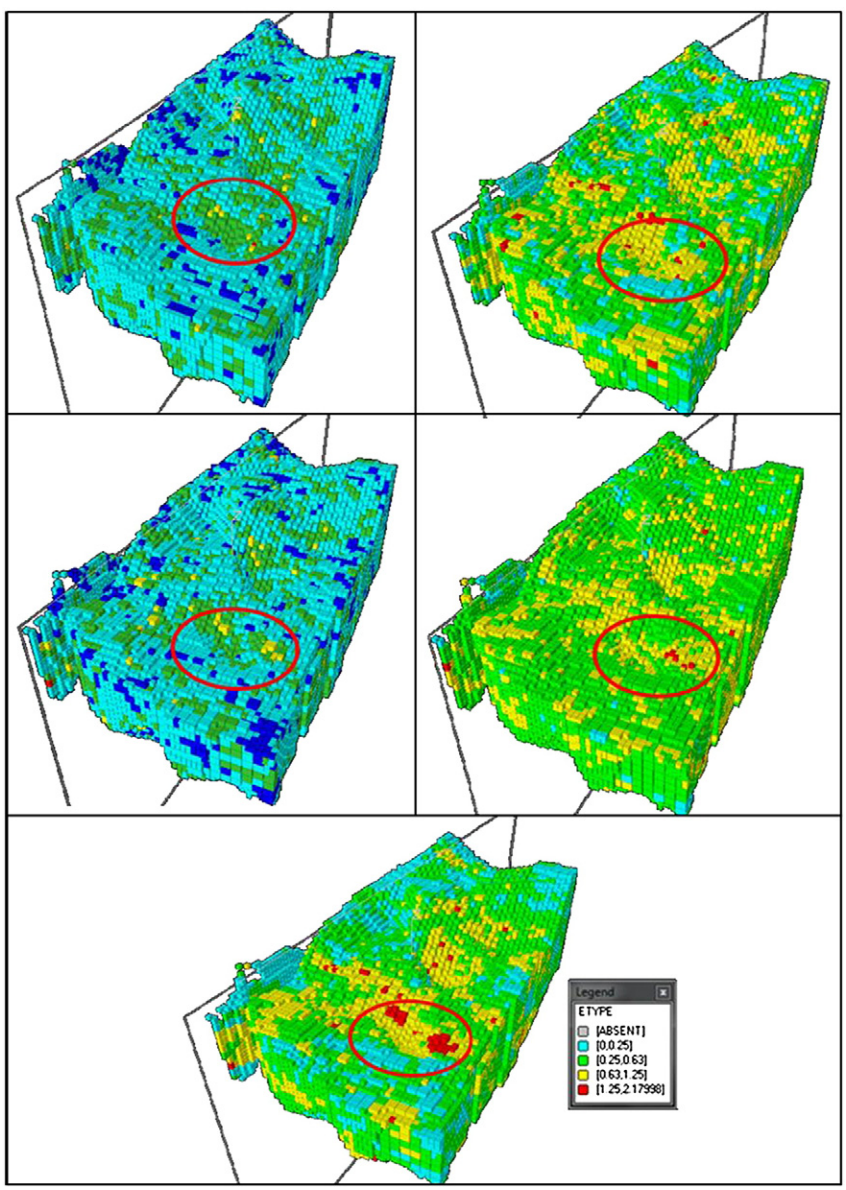

Fig. 8. Different Cu populations based on C–V multifractal modeling in different sim and E-type in the hypogene zone of the Sungun deposit.

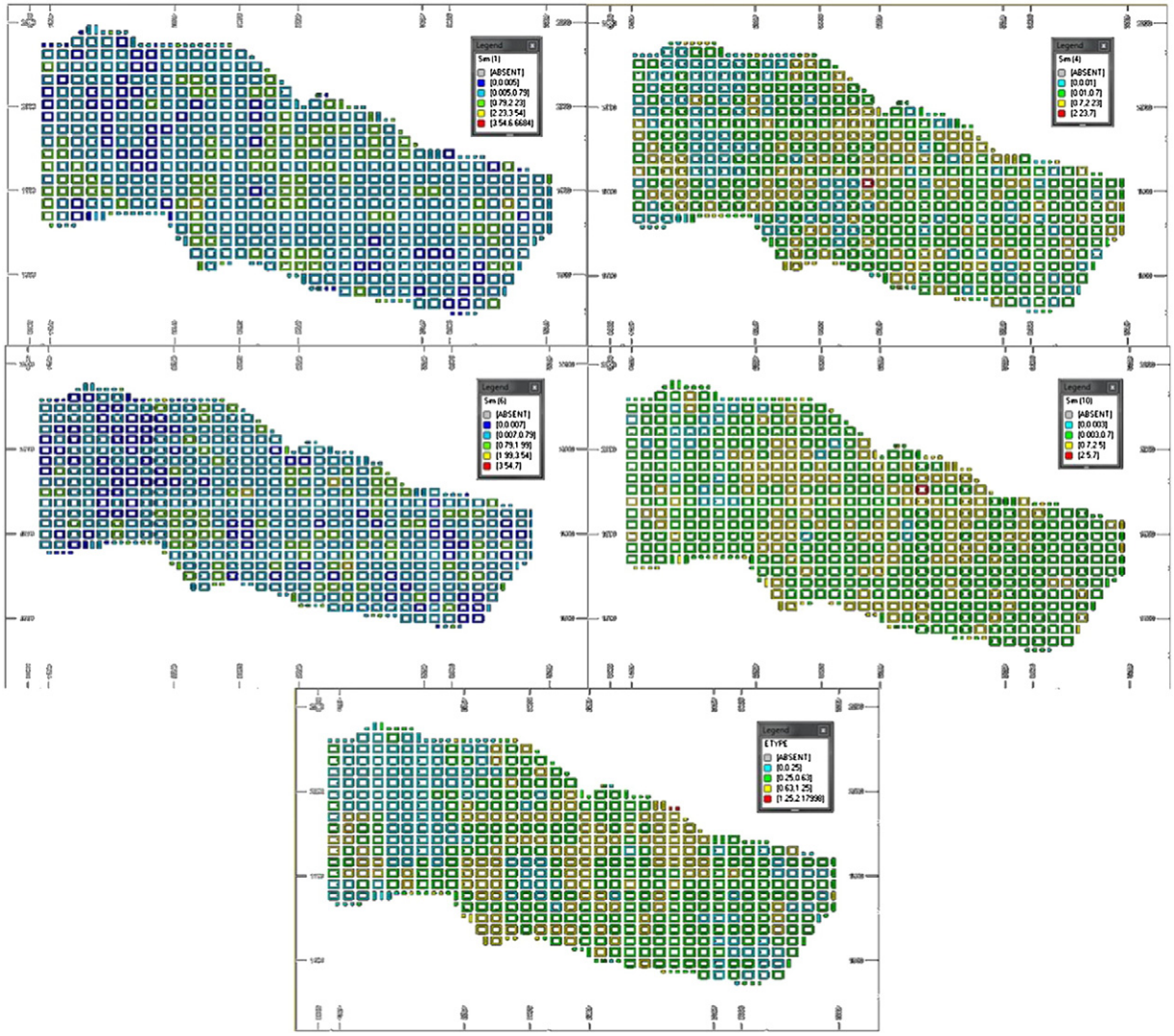

Fig. 8 (*continued*).

Based on the C–V modeling, 3D models of hypogene zone were generated in different realizations (Fig. 9). Some voxels with Cu high grade (>2.23% or >3.54%) are located in the upper parts of the hypogene zone and can be classified in the supergene enrichment zone. The propylitic alteration zone is a barren or weakly mineralized zone in the porphyry deposits (Berger et al., 2008; Lowell and Guilbert, 1970). According to the C–V fractal modeling on the results of SGS results, the Cu values of the alteration zone can be lower than 0.01% (sims 3, 4 and 7), 0.003% (sims 8 and 10), 0.005% (sims 1, 5 and 9), 0.007% (sims 2 and 6) and 0.25% (E-type).

Based on the Lowell and Guilbert (1970) model, potassic alteration zone occurs in the central part of the Cu porphyry deposits and hosts of high grade Cu mineralization. Based on C–V fractal modeling, potassic alteration has Cu values higher than 2.23% and 3.54% in different realizations and also Cu values higher than 1.26% can indicate potassic alteration zone due to E-type data (Table 3).

7. Comparison of fractal and alteration models of the deposit

Results of C–V modeling of the different realizations and E-type are correlated with the 3D alteration zone models of the hypogene zone of Sungun deposit consisting of potassic, phyllic and propylitic zones. These were generated by utilizing RockWorks™ v. 15 software and geological drillcore data (Fig. 10).

Carranza (2011) has illustrated an analysis for calculation of spatial correlations between two binary especially mathematical and geological models. An intersection operation between results derived via C–V fractal model and different alteration zones in the geological model (Table 3) was performed to obtain the numbers of voxels corresponding to each of the four classes of overlap zones as shown in Table 3. Utilizing the obtained numbers of voxels, Type I error (T1E), Type II error (T2E), and overall accuracy (OA) of the fractal model were estimated with respect to different alteration zones due to geological data (Carranza, 2011).

Based on C–V fractal modeling in different simulations (sims), propylitic alteration zone was correlated with Cu values lower than 0.01%, 0.003%, 0.005%, 0.007% and 0.25% (Table 3). Comparison between the alteration zone obtained from 3D geological modeling and the Cu thresholds from the C–V fractal modeling reveals that the propylitic zone is overlapped with the Cu values lower than 0.005% (sims 1, 5 and 9) more than the other results because of the fact that OA in the threshold (0.94) is higher than the others, as shown in Table 3. However, the OA between the alteration zone and C–V fractal modeling obtained by E-type data has a low value (0.7). Overall accuracies of the phyllic alteration zone with respect to the results of the fractal modeling of sim are between 0.36 and 0.59, but which indicate that the phyllic zone gives better results to recognize Cu values between 0.25 and 0.63% due to C–V modeling on E-type data in the deposit (Table 4).

Table 3
Matrix for comparing performance of fractal modeling results with geological model. A, B, C, and D represent numbers of voxels in overlaps between classes in the binary geological model and the binary results of fractal models (Carranza, 2011). OA, T1E and T2E with respect to propylitic alteration zone resulted from geological model and first threshold values of Cu obtained through C–V fractal modeling of different realizations and E-type in the hypogene zone.

		Geological model			
		Inside zone		Outside zone	
Fractal model	Inside zone	True positive (A)		False positive (B)	
	Outside zone	False negative (C)		True negative (D)	
		Type I error = C / (A + C)		Type II error = B / (B + D)	
		Overall accuracy = (A + D) / (A + B + C + D)			
		Propylitic alteration of geological model			
		Inside zones		Outside zones	
C–V fractal model of sims 1, 5 and 9 (Cu < 0.005%)	Inside zones	A	8	B	148
	Outside zones	C	8	D	3558
		T1E	0.9069	T2E	0.03993
		OA		0.9404	
C–V fractal model of sims 3, 4 and 7 (Cu < 0.01%)	Inside zones	A	25	B	333
	Outside zones	C	86	D	3348
		T1E	0.7747	T2E	0.0904
		OA		0.8895	
C–V fractal model of sims 2 and 6 (Cu < 0.007%)	Inside zones	A	13	B	220
	Outside zones	C	98	D	3461
		T1E	0.8828	T2E	0.0597
		OA		0.9161	
C–V fractal model of sims 8 and 10 (Cu < 0.003%)	Inside zones	A	14	B	263
	Outside zones	C	97	D	3418
		T1E	0.8738	T2E	0.0714
		OA		0.9050	
C–V fractal model of E-type (Cu < 0.25%)	Inside zones	A	39	B	842
	Outside zones	C	72	D	2839
		T1E	0.6486	T2E	0.2287
		OA		0.7589	

A comparison between C–V fractal modeling of sim and the potassic alteration zone in the 3D geological model indicates that high value of OA (0.816) exists between Cu values higher than 2.23% (sims 1, 5 and 9) and potassic alteration zone, as shown in Table 5. The correlation shows that the results obtained by sims 1, 5 and 9 are proper for the separation of potassic and propylitic alterations, but threshold values obtained from C–V fractal modeling based on the E-type data are more proper than the other realizations.

Moreover, correlation between geological data and results obtained by C–V fractal model represents a cross-section (Fig. 10). There is spatial coincidence between alteration zones defined by the C–V and SGS modeling and the zones defined by modeling of geological drillcore data. The propylitic alteration derived via C–V and SGS modeling occurs in marginal parts of the area which has good correlation with geological data in the southern part of the section. However, potassic alteration obtained by SGS and C–V modeling is situated in the central part of a cross-section which confirmed the geological data (Fig. 10).

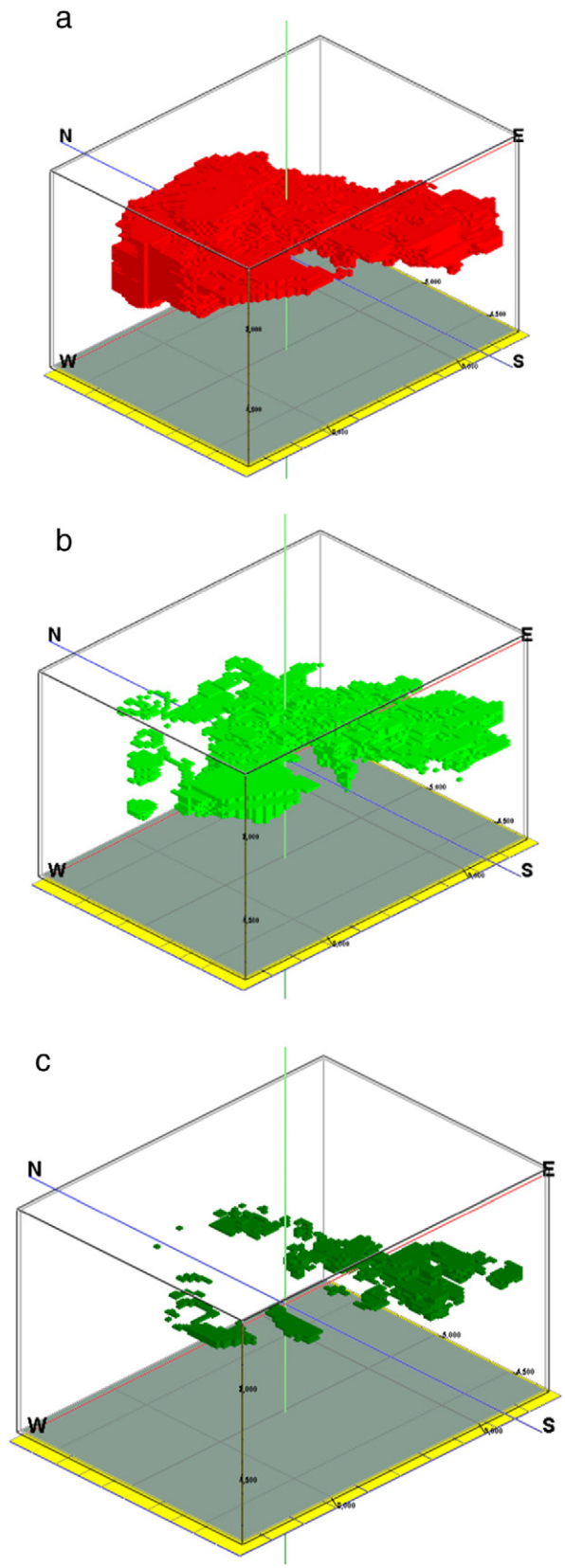

Fig. 9. Alteration zones in the hypogene zone of the Sungun deposit based on geological model: a) phyllic; b) potassic and c) propylitic.

8. Conclusion

Conventional geological modeling based on drillcore data is fundamentally essential for the determination of ore zone spatial structures, but ore grades are not observed in the methods. The ore grade variations in an ore deposit are obvious and salient features. Given the problems as mentioned above, using a series of mathematical analyses such as geostatistical simulation and fractal modeling seems to be inevitable. In many cases, drillcore logging in the geological study deals with the lack of proper diagnosis of geological phenomenon to identify alteration

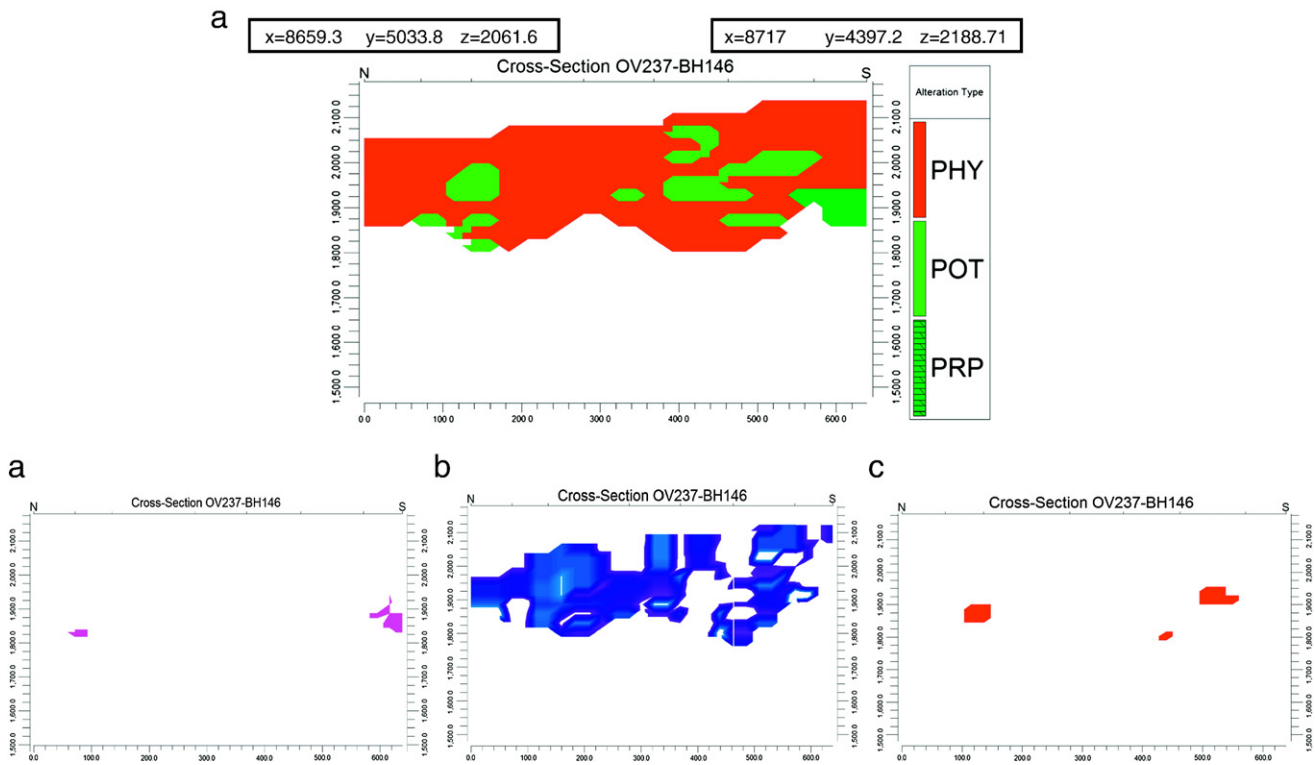

Fig. 10. Representative cross-sections of alteration zones: (a) based on 3D modeling of drillcore geological data; (b) C–V modeling of sims 1, 5, and 9 (Cu < 0.005%: propylitic); (c) C–V modeling of E-type (0.25 < Cu < 0.63%: phyllic) and (d) C–V modeling of sims 1, 5, and 9 (Cu > 2.23%: potassic).

Table 4
OA, T1E and T2E with respect to phyllic alteration zone resulted from geological model and threshold values of Cu obtained through C–V fractal modeling of different realizations and E-type in the hypogene zone.

		Phyllic alteration of geological model			
		Inside zones		Outside zones	
C–V fractal model of E-type (0.25% < Cu < 0.63%)	Inside zones	A	895	B	279
	Outside zones	C	843	D	1775
		T1E	0.4850	T2E	0.1358
		OA		0.7041	
C–V fractal model of E-type (0.63% < Cu < 1.26%)	Inside zones	A	287	B	106
	Outside zones	C	1451	D	1948
		T1E	0.8348	T2E	0.0516
		OA		0.5893	
C–V fractal model of sims 1, 5 and 9 (0.005% < Cu < 0.79%)	Inside zones	A	1918	B	598
	Outside zones	C	925	D	351
		T1E	0.3253	T2E	0.6301
		OA		0.5983	
C–V fractal model of sims 1, 5 and 9 (0.79% < Cu < 2.23%)	Inside zones	A	652	B	207
	Outside zones	C	2191	D	742
		T1E	0.7706	T2E	0.2181
		OA		0.3676	
C–V fractal model of sims 1, 5 and 9 (2.23% < Cu < 3.54%)	Inside zones	A	8	B	2
	Outside zones	C	2835	D	947
		T1E	0.9971	T2E	0.0021
		OA		0.2518	
C–V fractal model of sims 3, 4 and 7 (0.01% < Cu < 0.7%)	Inside zones	A	1874	B	873
	Outside zones	C	969	D	76
		T1E	0.3408	T2E	0.9199
		OA		0.5142	

zones due to a series of established modeling based on mathematical analyses such as geostatistical simulation and fractal modeling. The Gaussian simulations honor the covariance models of the data point and that is why they are appropriate for modeling of processes with extreme large continuity. The SGS is useful in generating relatively various

Table 5
OA, T1E and T2E with respect to potassic alteration zone resulted from geological model and threshold values of Cu obtained through C–V fractal modeling of different realizations and E-type in the hypogene zone.

		Potassic alteration of geological model			
		Inside zones		Outside zones	
C–V fractal model of E-type (1.26% < Cu)	Inside zones	A	3	B	14
	Outside zones	C	697	D	3078
		T1E	0.9957	T2E	0.0045
		OA		0.8125	
C–V fractal model of sims 1, 5 and 9 (2.23% < Cu)	Inside zones	A	4	B	1
	Outside zones	C	696	D	3091
		T1E	0.9942	T2E	0.0003
		OA		0.8162	
C–V fractal model of sims 1, 5 and 9 (3.54% < Cu)	Inside zones	A	1	B	1
	Outside zones	C	699	D	3091
		T1E	0.9985	T2E	0.0003
		OA		0.8154	
C–V fractal model of sims 1, 5 and 9 (0.79% < Cu < 2.23%)	Inside zones	A	159	B	570
	Outside zones	C	541	D	2522
		T1E	0.7728	T2E	0.1843
		OA		0.7070	
C–V fractal model of E-type (0.63% < Cu < 1.26%)	Inside zones	A	189	B	652
	Outside zones	C	511	D	2440
		T1E	0.73	T2E	0.2108
		OA		0.6933	

realizations in the ore deposits, where computational efficiency and effective implementation are important.

In this paper, the SGS and C–V fractal models were utilized to delineate different alteration zones in the hypogene zone of Sungun Cu porphyry deposit, NW Iran. Investigation of the deposit indicates that the results derived via geostatistical simulations can be used for the separation of alteration zones by fractal modeling. Furthermore, the three realizations (sims 1, 5 and 9) show the proper results for delineation of potassic and propylitic alteration zones. Moreover, C–V modeling on E-type data is suitable for phyllic alteration. On the other hand, C–V fractal modeling based on E-type data is proper for moderate Cu values.

Correlation between results and alteration zones obtained by geological model of the hypogene zone reveals that propylitic alteration has Cu values lower than 0.005% and potassic alteration zone correlated with Cu values higher than 2.23%. There is a good relationship between phyllic alteration zone and Cu values between 0.25% and 0.63% derived by E-type data. Moreover, the voxels with high values of Cu (>3.54%) which exist in upper levels of the hypogene zone can be classified in supergene enrichment zone of the deposit. Furthermore, the obtained results strongly support the Lowell and Guilbert (1970) model for alteration zones of porphyry copper deposits.

Acknowledgments

The authors would like to thank Mr. Amir Bijan Yasrebi from Camborne School of Mines for his remarkable contribution. The authors would like to thank the editors and reviewers of this paper for their comments and valuable remarks.

References

Afzal, P., Fadakar Alghalandis, Y., Khakzad, A., Moarefvand, P., Rashidnejad Omran, N., 2011. Delineation of mineralization zones in porphyry Cu deposits by fractal concentration–volume modeling. J. Geochem. Explor. 108, 220–232.

Afzal, P., Fadakar Alghalandis, A., Moarefvand, P., Rashidnejad Omran, N., Asadi Haroni, H., 2012. Application of power–spectrum–volume fractal method for detecting hypogene, supergene enrichment, leached and barren zones in Kahang Cu porphyry deposit, Central Iran. J. Geochem. Explor. 112, 131–138.

Afzal, P., Dadashzadeh Ahari, H., Rashidnejad Omran, N., Aliyari, F., 2013. Delineation of gold mineralized zones using concentration–volume fractal model in Qolqoleh gold deposit, NW Iran. Ore Geol. Rev. 55, 125–133.

Agterberg, F.P., 1995. Multifractal modeling of the sizes and grades of giant and supergiant deposits. Int. Geol. Rev. 37, 1–8.

Arias, M., Gumiel, P., Martín-Izard, C., 2012. Multifractal analysis of geochemical anomalies: a tool for assessing prospectivity at the SE border of the Ossa Morena Zone, Variscan Massif (Spain). J. Geochem. Explor. 122, 101–112.

Asghari, O., Hezarkhani, A., 2008. Appling discriminant analysis to separate the alteration zones within the Sungun porphyry copper deposit. Asian J. Appl. Sci. 8 (24), 4472–4486.

Asghari, O., Madani Esfahani, N., 2013. A new approach for the geological risk evaluation of coal resources through a geostatistical simulation. Arab. J. Geosci. 6, 929–943.

Asghari, O., Hezarkhani, A., Soltani, F., 2009. The comparison of alteration zones in the Sungun porphyry copper deposit, Iran (based on fluid inclusion studies). Acta Geol. Pol. 59 (1), 93–109.

Berberian, M., King, G.C., 1981. Towards a paleogeography and tectonic evolution of Iran. Can. J. Earth Sci. 18, 210–265.

Bloorn, M.S., 1981. Chemistry of inclusion fluids: stockwork molybdenum deposits from Questa, New Mexico, and Hudson Bay Mountain and Endako, British Columbia. Econ. Geol. 76, 1906–1920.

Berger, B.R., Ayuso, R.A., Wynn, J.C., Seal, R.R., 2008. Preliminary model of porphyry copper deposits. USGS, Open-file Report (1321 pp.).

Calagari, A.A., 2004. Fluid inclusion studies in quartz veinlets in the porphyry copper deposit at Sungun, East-Azerbaijan, Iran. J. Asian Earth Sci. 23, 179–189.

Carranza, E.J.M., 2009. Controls on mineral deposit occurrence inferred from analysis of their spatial pattern and spatial association with geological features. Ore Geol. Rev. 35, 383–400.

Carranza, E.J.M., 2011. Analysis and mapping of geochemical anomalies using logratio-transformed stream sediment data with censored values. J. Geochem. Explor. 110, 167–185.

Carranza, E.J.M., Sadeghi, M., 2010. Predictive mapping of prospectivity and quantitative estimation of undiscovered VMS deposits in Skellefte district (Sweden). Ore Geol. Rev. 38, 219–241.

Chen, F., Sh, Chen, Peng, G., 2013. Using Sequential Gaussian Simulation to assess geochemical anomaly areas of lead element, computer and computing technologies in agriculture VI IFIP advances. Information and Communication Technology, vol. 393, pp. 69–76.

Cheng, Q., 1999. Spatial and scaling modelling for geochemical anomaly separation. J. Geochem. Explor. 65 (3), 175–194.

Cheng, Q., Agterberg, F.P., Ballantyne, S.B., 1994. The separation of geochemical anomalies from background by fractal methods. J. Geochem. Explor. 51, 109–130.

Chilès, J.-P., Delfiner, P., 2012. Geostatistics: Modeling Spatial Uncertainty, 2nd edition. Wiley 734.

Chouinard, A., Williams-Jones, A.E., Leonardson, R.W., Hodgson, C.J., 2005. Geology and genesis of the multistage high sulfidation epithermal Pascua Au–Ag–Cu deposit, Chile and Argentina. Econ. Geol. 100, 463–490.

Cox, D., Singer, D., 1986. Mineral deposits models. U.S. Geological Survey Bulletin (1693 pp.).

Daneshvar Saein, L., Rasa, I., Rashidnejad Omran, N., Moarefvand, P., Afzal, P., 2012. Application of concentration–volume fractal method in induced polarization and resistivity data interpretation for Cu–Mo porphyry deposits exploration, case study: Nowchun Cu–Mo deposit, SE Iran. Nonlinear Process. Geophys. 19, 431–438.

Dargahi, S., Arvin, M., Pan, Y., Babaei, A., 2010. Petrogenesis of post-collisional A-type granitoid from the Urumieh–Dokhtar magmatic assemblage, Southwestern Kerman, Iran: constraints on the Arabian–Eurasian continental collision. Lithos 115, 190–204.

Delavar, S.T., Afzal, P., Borg, G., Rasa, I., Lotfi, M., Rashidnejad Omran, N., 2012. Delineation of mineralization zones using concentration–volume fractal method in Pb–Zn carbonate hosted deposits. J. Geochem. Explor. 118, 98–110.

Delbari, M., Afrasiab, P., Loiskandl, W., 2009. Using Sequential Gaussian Simulation to assess the field-scale spatial uncertainty of soil water content. Catena 79, 163–169.

Deutsch, C., Journel, A.G., 1998. GSLIB: Geostatistical Software Library and User's Guide Second Edition. Oxford University Press, New York (340 pp.).

Dimitrakopoulos, R., Luo, X., 2004. Generalized Sequential Gaussian Simulation on group size ν and screen-effect approximations for large field simulations. Math. Geol. 36, 567–591.

Emery, X., Peláez, M., 2012. Assessing the accuracy of Sequential Gaussian Simulation and cosimulation. Comput. Geosci. 15, 673–689.

Geboy, N.J., Olea, R.A., Engle, M.A., Martín-Fernández, J.A., 2013. Using simulated maps to interpret the geochemistry, formation and quality of the Blue Gem coal bed, Kentucky, USA. Int. J. Coal Geol. 112, 26–35.

Goncalves, M.A., Mateus, A., Oliveira, V., 2001. Geochemical anomaly separation by multifractal modeling. J. Geochem. Explor. 72, 91–114.

Goovaerts, P., 1996. Stochastic simulation of categorical variables using a classification algorithm and simulated annealing. Math. Geol. 28, 909–921.

Goovaerts, P., 1997. Geostatistics for Natural Resources Evaluation. Oxford University Press, New York (483 pp.).

Gumiel, P., Sanderson, D.J., Arias, M., Roberts, S., Martín-Izard, A., 2010. Analysis of the fractal clustering of ore deposits in the Spanish Iberian Pyrite Belt. Ore Geol. Rev. 38–4, 307–318.

Hassanpour, Sh., Afzal, P., 2013. Application of concentration–number (C–N) multifractal modelling for geochemical anomaly separation in Haftcheshmeh porphyry system, NW Iran. Arab. J. Geosci. 6, 957–970.

Hedenquist, J.W., Arribas, R.A., Gonzalez-Urien, E., 2000. Exploration for epithermal gold deposits. In: Hagemann, S.G. (Ed.), Gold in 2000. Rev. Econ. Geol., 13, pp. 245–277.

Hezarkhani, A., 2006. Petrology of intrusive rocks within the Sungun porphyry copper deposit, Azerbaijan, Iran. J. Asian Earth Sci. 73, 326–340.

Hezarkhani, A., Williams-Jones, A.E., 1998. Controls of alteration and mineralization in the Sungun porphyry copper deposit, Iran: evidence from fluid inclusions and stable isotopes. Econ. Geol. 93, 651–670.

Hezarkhani, A., Williams-Jones, A.E., Gammons, C.H., 1999. Factors controlling copper solubility and chalcopyrite deposition in the Sungun porphyry copper deposit, Iran. Mineral. Deposita 34, 770–783.

Hoefs, J., 2009. Stable Isotope Geochemistry. Springer-Verlag Berlin Heidelberg, Berlin.

Isaaks, E.H., Srivastava, R.M., 1989. An Introduction to Applied Geostatistics. Oxford University Press, New York (561 pp.).

Journel, A.G., 1993. Modeling Uncertainty: Some Conceptual Thoughts, Geostatistics for the Next Century. Kluwer Academic Publications 30–43.

Journel, A.G., Huijbregts, C.J., 1978. Mining Geostatistics. Academic Press, New York (600 pp.).

Leuangthong, O., McLennan, J.A., Deutsch, C.V., 2004. Minimum acceptance criteria for geostatistical realizations. Nat. Resour. Res. 13, 131–141.

Li, C., Ma, T., Shi, J., 2003. Application of a fractal method relating concentrations and distances for separation of geochemical anomalies from background. J. Geochem. Explor. 77, 167–175.

Lowell, J.D., Guilbert, J.M., 1970. Lateral and vertical alteration–mineralization zoning in porphyry ore deposits. Econ. Geol. 65, 373–408.

Maleki Tehrani, M.A., Asghari, O., Emery, X., 2012. Simulation of mineral grades and classification of mineral resources by using hard and soft conditioning data: application to Sungun porphyry copper deposit. Arab. J. Geosci. http://dx.doi.org/10.1007/s12517-012-0638-y.

Manchuk, J.G., Deutsch, C.V., 2012a. Implementation aspects of Sequential Gaussian Simulation on irregular points. Comput. Geosci. 16 (3), 625–637.

Manchuk, J.G., Deutsch, C.V., 2012b. A flexible Sequential Gaussian Simulation program: USGSIM. Comput. Geosci. 41, 208–216.

Mandelbrot, B.B., 1983. The Fractal Geometry of Nature. W. H. Freeman, San Francisco.

Mehrpartou, M., 1993. Contributions to the geology, geochemistry, ore genesis and fluid inclusion investigations on Sungun Cu–Mo porphyry deposit, northwest of Iran. Unpublished PhD Thesis. University of Hamburg, Germany, p. 245.

Parsolang Engineering Consultant, 2006. Company, Parsolang Modeling and Reserve Estimation Report of Sungun Copper Mine, Tehran.

Pirajno, F., 2009. Hydrothermal Processes and Mineral Systems. Springer, The University of Western Australia, Perth.

Qu, M., Li, W., Zhang, Ch., 2013. Assessing the risk costs in delineating soil nickel contamination using Sequential Gaussian Simulation and transfer functions. Ecological Informatics, vol. 13, pp. 99–105 (January).

Rashidinejad, F., Osanloo, M., Rezai, B., 2008. Cut of grades optimization with environmental management; a case study: Sungun Copper Porphyry Project, IUST. Int. J. Eng. Sci. 19, 1–13.

Ravenscroft, P.J., 1994. Conditional simulation for mining: practical implementation in an industrial environment. In: Armstrong, M., Dowd, P.A. (Eds.), Geostatistical Simulations. Kluwers, Dordrecht, pp. 79–87.

Rezaee, H., Mariethoz, G., Koneshloo, M., Asghari, O., 2013. Multiple-point geostatistical simulation using the bunch-pasting direct sampling method. Comput. Geosci. 54, 293–308.

Richards, J.P., 1995. Alkalic-type epithermal gold deposits. Mineralogical Association of Canada Short Course Handbook, 23 367–400.

Sadeghi, B., Moarefvand, P., Afzal, P., Yasrebi, A.B., Daneshvar Saein, L., 2012. Application of fractal models to outline mineralized zones in the Zaghia iron ore deposit, Central Iran. J. Geochem. Explor. 122, 9–19.

Sillitoe, R.H., 1997. Characteristics and controls of the largest porphyry copper–gold and epithermal gold deposits in the circum-pacific region. Aust. J. Earth Sci. 44, 373–388.

Sim, B.L., Agterberg, F.P., Beaudry, C., 1999. Determining the cutoff between background and relative base metal contamination levels using multifractal methods. Comput. Geosci. 25, 1023–1041.

Wang, Q.F., Deng, J., Liu, H., Wang, Y., Sun, X., Wan, L., 2011. Fractal models for estimating local reserves with different mineralization qualities and spatial variations. J. Geochem. Explor. 108, 196–208.

Yasrebi, A.B., Afzal, P., Wetherelt, A., Foster, P., Esfahanipour, R., 2013. Correlation between geological and concentration–volume fractal models for Cu and Mo mineralised zones separation in Kahang Porphyry Deposit, Central Iran. Geol. Carpath. 64 (2), 153–163.

Zanon, S., Leuangthong, O., 2004. Implementation aspects of sequential simulation. In: Leuangthong, O., Deutsch, C. (Eds.), Geostatistics Banff, vol. 1. Springer Science + Business Media, pp. 543–550.

Zuo, R., 2011. Identifying geochemical anomalies associated with Cu and Pb–Zn skarn mineralization using principal component analysis and spectrum-area fractal modelling in the Gangdese Belt, Tibet (China). J. Geochem. Explor. 111, 13–22.

Zuo, R., Cheng, Q., Xia, Q., 2009. Application of fractal models to characterization of vertical distribution of geochemical element concentration. J. Geochem. Explor. 102, 37–43.